Calhoun

Institutional Archive of the Naval Postgraduate School

Calhoun: The NPS Institutional Archive

Faculty and Researcher Publications   Faculty and Researcher Publications

2006

Comparison of methods for deriving aerosol asymmetry parameter

Andrews, E.

http://hdl.handle.net/10945/42228

Comparison of methods for deriving aerosol asymmetry parameter

E. Andrews,[1] P. J. Sheridan,[2] M. Fiebig,[3,4] A. McComiskey,[1] J. A. Ogren,[2] P. Arnott,[5] D. Covert,[6] R. Elleman,[6] R. Gasparini,[7,8] D. Collins,[7] H. Jonsson,[9] B. Schmid,[10] and J. Wang[11]

[1] Values for Mie-equivalent aerosol asymmetry parameter (g) were derived using a variety of methods from the large suite of measurements (in situ and remote from surface and aircraft) made in Oklahoma during the 2003 aerosol Intensive Operations Period (IOP). Median values derived for dry asymmetry parameter at 550 nm ranged between 0.55 and 0.63 over all instruments and for all derivation methods, with the exception of one instrument which did not measure over the full size range of optically important aerosol. Median values for the "wet" asymmetry parameter (i.e., asymmetry parameter at humidity conditions closer to ambient) were between 0.59 and 0.72. Values for g derived for surface and airborne in situ measurements were highly correlated, but in situ and remote sensing measurements both at the surface and aloft did not agree as well because of vertical inhomogeneity of the aerosol. Radiative forcing calculations suggest that a 10% decrease in g would result in a 19% reduction in top of atmosphere radiative forcing for the conditions observed during the IOP. Comparison of the different methods for deriving g suggests that in computing the asymmetry parameter, aerosol size is the most important parameter to measure; composition is less important except for how it influences the hygroscopic growth (i.e., size) of particles.

1. Introduction

[2] Radiative forcing by aerosol particles can be an important contributor to climate change but the magnitude, as well as the sign of the forcing effect, is highly uncertain [*Intergovernmental Panel on Climate Change*, 2001]. The angular distribution of light scattered by aerosol particles (i.e., the aerosol phase function) is one of the key properties controlling the aerosol contribution to forcing and depends on the size and composition of the particles. Radiative transfer models commonly utilize a parameterization of the angular distribution of scattered light because such parameterizations are computationally more efficient than computing aerosol phase functions in already complex radiative transfer codes. Some simple, single-valued representations of the angular scattering include the asymmetry parameter (g), the upscatter fraction (β) and the hemispheric backscatter fraction (b).

[3] Each of these representations of angular scattering is useful in different applications. The hemispheric backscatter fraction is a parameter that can be continuously measured in the field by an integrating nephelometer equipped with backscatter shutter [*Charlson et al.*, 1974]. The measurements of b are often transformed to β and combined with other in situ measurements to calculate radiative forcing for a specific local aerosol [e.g., *Delene and Ogren*, 2002]. More generally a reasonable value for upscatter fraction β is assumed and used in some simplified radiative forcing equations to determine top of atmosphere (TOA) forcing [*Haywood and Shine*, 1995; *Charlson et al.*, 1991]. The asymmetry parameter is commonly used in large-scale radiative transfer models via the Henyey-Greenstein phase function or the Eddington approximation which depend on the value of g [e.g., *Boucher*, 1998].

[4] Several researchers [*Wiscombe and Grams*, 1976; *Marshall et al.*, 1995] have investigated relationships among b, β and g with the idea of simplifying the process of going from a measured quantity (e.g., b) to quantities used in radiative forcing calculations. They note that unlike the smooth functions derived using the Henyey-Greenstein approximation, there is not a unique relationship between

[1]Cooperative Institute for Research in Environmental Sciences, University of Colorado, Boulder, Colorado, USA.

[2]Global Monitoring Division, NOAA Earth System Research Laboratory, Boulder, Colorado, USA.

[3]Visiting Scientist at Global Monitoring Division, NOAA Earth System Research Laboratory, Boulder, Colorado, USA.

[4]Now at Institut für Physik der Atmosphäre, Deutsches Zentrum für Luft- und Raumfahrt Oberpfaffenhofen, Wessling, Germany.

[5]Desert Research Institute, Reno, Nevada, USA.

[6]Department of Atmospheric Sciences, University of Washington, Seattle, Washington, USA.

[7]Department of Atmospheric Sciences, Texas A&M University, College Station, Texas, USA.

[8]Now at Source Environmental Sciences, Inc., Houston, Texas, USA.

[9]Center for Interdisciplinary Remotely-Piloted Aircraft Studies, Naval Postgraduate School, Marina, California, USA.

[10]Bay Area Environmental Research Institute, Sonoma, California, USA.

[11]Brookhaven National Laboratory, Upton, New York, USA.

backscattered fraction and the asymmetry parameter calculated using more realistic Mie theory. The multivalued relationship between g and b (and β) is problematic for at least two reasons: (1) Simple parameterizations of a measured quantity b cannot always be used to determine the "correct" value for g, and (2) algorithms which use different functional dependences for g cannot be directly compared, adding to uncertainty in model intercomparisons.

[5] Because g is a fundamental parameter for radiative transfer, we choose to focus on the uncertainties in the derivation of asymmetry parameter from a diverse range of aerosol measurements. The asymmetry parameter (g) is defined as the intensity-weighted average cosine of the scattering angle:

$$g = \frac{1}{2} \int_0^\pi \cos\theta P(\theta) \sin\theta d\theta \qquad (1)$$

where θ is the angle between incident light and scattering direction and P(θ) is the angular distribution of scattered light (the phase function). The value of g ranges between -1 for entirely backscattered light to $+1$ for entirely forward scattered light.

[6] Typically, radiative forcing models have either assumed some relationship between b (or β) [*Wiscombe and Grams*, 1976] and g or relied on look-up table parameterizations of aerosol optical properties such as *d'Almeida et al.* [1991] and *Hess et al.* [1998]. These parameterizations are based on assumed aerosol sizes and compositions for different idealized aerosol types. *D'Almeida et al.* [1991] suggest a range in g for dry aerosol particles at 500 nm wavelength between 0.64 and 0.83 depending on the aerosol type and season, with a average value over all aerosol types being approximately 0.72. For high relative humidity the average value for g over all aerosol types increases to approximately 0.79 with a range $0.64-0.82$. Global maps of asymmetry parameter presented by *d'Almeida et al.* [1991] suggest a value for g of 0.67 at ambient relative humidity (RH) for most of the midwest and south east regions of the US where the measurements discussed here were carried out.

[7] Phase functions for individual particles have been measured in the lab [e.g., *Volten et al.*, 2001] and from such observations g can be directly calculated from the fundamental definition of g (equation (1)). Unfortunately, there is no commercially available instrument for directly measuring aerosol g in the atmosphere. Cloud integrating nephelometers [*Gerber et al.*, 2000] and polar nephelometers [e.g., *Gayet et al.*, 1998] have been used to obtain g for cloud drops and ice crystals but these techniques have not typically been used to obtain g for aerosol because of limitations with signal intensity and light source stability [*Leong et al.*, 1995]. *Heintzenberg and Charlson* [1996] describe the state of the art of integrating nephelometry measurements and discuss both the need for and modifications to an integrating nephelometer for making asymmetry parameter measurements. Typically then, in field observations, values for asymmetry parameter must be derived from other aerosol measurements rather than direct observation. Because there are many types of measurements that can be used to derive g and consequently a variety of assumptions and uncertainties that go into the derivation, an intercom-

parison can provide insight into how well g can be estimated with each measurement method. Additionally, the sensitivity of derived values of g to various aerosol properties (e.g., composition or size distribution) can be evaluated.

[8] In May 2003 a multi-instrument, multiplatform experiment occurred to measure various aerosol properties relevant to aerosol radiative forcing at a midlatitude continental site. Here, measurements from this experiment are used to answer the following questions:

[9] 1. What is the range of values for g at this site? How does this range affect calculations of aerosol forcing?

[10] 2. How much do these values vary depending on the instruments and methods used to derive them?

[11] 3. Are the values of g observed consistent with other indicators of aerosol type?

[12] 4. What is the effect of relative humidity on the range of g?

[13] 5. On the basis of the range of aerosol properties observed during the experiment, what aerosol properties are most important to measure to obtain a well-constrained value of g?

[14] 6. Are there any significant differences in the estimate of g for surface-based versus vertical profile (column) measurements?

[15] 7. Are the g values observed during this study typical of conditions at the site?

2. Methods

[16] The Aerosol Intensive Observational Period (IOP) occurred $5-31$ May 2003 at the Department of Energy's (DOE) Cloud and Radiation Testbed (CART) Southern Great Plains (SGP) Central Facility near Lamont, Oklahoma (36.6 N, 97.5 W, 315 m asl). The main purpose of the IOP was to improve understanding and representation of aerosol radiative properties in models. To this end, a variety of platforms and instruments were deployed to measure the physical, chemical and optical properties of aerosol particles at SGP, in addition to the suite of measurements made at the site on an ongoing basis. The campaign and the associated measurements are described by *Ferrare et al.* [2006]. The measurements relevant to the derivation of asymmetry parameter are listed in Table 1 and described in detail below, segregated by measurement type (in situ or remote) and location (surface and airborne). The methods used to derive asymmetry parameter from the measurements are outlined following the instrumentation descriptions. To verify our approach, we compared measured and calculated aerosol light scattering using Mie theory directly or data inversion (which indirectly relies on Mie theory) as appropriate to check the instruments and our calculation techniques. While good agreement between measured and derived scattering does not necessarily imply that we are modeling the aerosol correctly, it does nonetheless give us confidence that the independent data sets are consistent.

2.1. Surface Aerosol Instrumentation

[17] As part of the long-term aerosol measurements at the SGP CART site (since 1996), NOAA's Climate Monitoring and Diagnostics Laboratory (CMDL) has mentored an "Aerosol Observing System" (AOS) which includes two 3-wavelength integrating nephelometers (Model#3563, TSI

Table 1. List of Instruments Used for Derivation of Asymmetry Parameter During IOP[a]

Instrument (Size Range)	Measurement	Method to Derive g	Investigator(s)
In Situ Measurements: Surface			
AOS nephelometer (<10 μm and <1 μm)	$\sigma_{sp}(\lambda), \sigma_{bsp}(\lambda)$	Henyey-Greenstein, Fiebig inversion	Ogren and Sheridan, NOAA/CMDL
AOS PCASP (0.10–10.0 μm)	dry aerosol size distribution	Mie calculations	Ogren and Sheridan, NOAA/CMDL
GIF SMPS (0.03–0.82 μm)	dry aerosol size distribution	Mie calculations	Wang, BNL
GIF TDMA (0.01–1.0 μm)	dry and wet aerosol size distribution and size-resolved hygroscopicity	Mie calculations	Gasparini and Collins, Texas A&M
GIF Climet (0.35–11.4 μm)	dry aerosol size distribution	Mie calculations	Arnott, DRI
In Situ Measurements: Aircraft			
IAP nephelometer (<1 μm)	$\sigma_{sp}(\lambda), \sigma_{bsp}(\lambda)$	Henyey-Greenstein	Ogren and Sheridan, NOAA/CMDL
TO nephelometer (no size cut)	$\sigma_{sp}(\lambda), \sigma_{bsp}(\lambda)$	Henyey-Greenstein	Covert and Elleman, University of Washington
TO PCASP (0.11–2.69 μm)	dry aerosol size distribution	Mie calculations	Jonsson, CIRPAS
TO SMPS (0.02–0.73 μm)	dry aerosol size distribution	Mie calculations	Wang, BNL
Remote Sensing Measurements			
AERONET[b] (no size cut)	AOD(λ)	Dubovik inversion	Bartholomew, AERONET
TO AATS (no size cut)	AOD(λ)	King inversion	Schmid, NASA/Ames and BAERI

[a]AOS, aerosol observing system; GIF, guest instrument facility; IAP, in situ aerosol profiling; TO, Twin Otter.
[b]At the surface.

Inc., St. Paul, Minnesota) with total and backscatter capabilities for dry and humidified aerosol light scattering measurements (both total scattering σ_{sp}, and backscattering σ_{bsp}), a particle soot absorption photometer (PSAP, Radiance Research, Seattle, Washington) for light absorption (σ_{ap}) measurements and a CN counter (Model#3010, TSI Inc., St. Paul, Minnesota). The nephelometers and PSAP are downstream of a 10 μm aerodynamic diameter impactor and every 6 min a 1 μm aerodynamic diameter impactor is switched into or out of the sample flow for 6 min. This results in sub-10 μm and sub-1 μm aerodynamic aerosols being sampled during alternating 6 min periods. The nephelometer measurements are corrected for angular nonidealities using the scheme described by *Anderson and Ogren* [1998], while the PSAP measurements are corrected using the *Bond et al.* [1999] algorithm. The AOS system and results from the first 4 years of measurements are described by *Sheridan et al.* [2001]. During the IOP, a mobile aerosol system with an additional nephelometer and PSAP at low-RH conditions was set up in the Guest Instrument Facility (GIF) trailer which was located approximately 150 m from the AOS trailer. This mobile aerosol rack was used for quality control both to check that the same aerosol was being sampled at the AOS and GIF trailers and as a transfer standard to intercompare other nephelometers and PSAPs deployed during the IOP. Additionally the GIF nephelometer and PSAP served as backup for the instruments in the AOS trailer. On the basis of calculations performed for the INDOEX campaign [*Clarke et al.*, 2002], the uncertainty in the nephelometer scattering measurements at the surface are about 10% of the total measured scattering.

[18] Also in the AOS trailer a passive cavity aerosol spectrometer probe (Model#PCASP-X, Particle Measuring Systems, Boulder, Colorado) measured aerosol number concentrations in 32 size bins between 0.1 and 10 μm (optical diameter). The AOS PCASP is calibrated with polystyrene latex spheres (refractive index, RI = 1.58) as described by *Liu et al.* [1992], response curves for other values of RI are calculated using Mie theory and a code modeling the PCASP [*Hand and Kreidenweis*, 1996]. Here we used diameters corresponding to the response curve calculated for RI = 1.55 + 0.015i. Particles in the 0.1–10 μm size range scatter light very effectively; a closure comparison of scattering (Figure 1) measured by the AOS low-RH nephelometer with scattering calculated from the PCASP size distributions using Mie theory shows excellent agreement (within 2% on the basis of the slope of a line forced through the origin, R^2 = 0.97) suggesting both instruments are sampling the optically important aerosol. This light scattering comparison is for a wavelength (λ) of 550 nm and assumes homogeneous spheres over the entire PCASP size range. The AOS PCASP instrument was only operational during the middle portion of the IOP, from 12 to 24 May 2003 (Day of year (DOY) 132–144). The light absorption calculated from measured size distributions for the same conditions (λ = 550 nm, RI = 1.55 + 0.015i) also showed good agreement with light absorption measured by the PSAP (within 3% on the basis of the slope of a line forced through the origin, R^2 = 0.43). The lower correlation coefficient for absorption shows that calculated absorption is more sensitive to the refractive index (particularly the imaginary part) and that the contribution of absorbing material to the aerosol is variable. Throughout this paper we report calculated optical properties at λ = 550 nm and RI = 1.55 + 0.015i unless otherwise noted.

[19] A humidity conditioning system and second nephelometer in the AOS trailer are used to measure light scattering and backscattering as a function of relative humidity. Over the course of an hour the humidity conditioning system generates a controlled scan of relative humidity, ideally increasing from approximately 40% up to 90%, although during the IOP the maximum RH
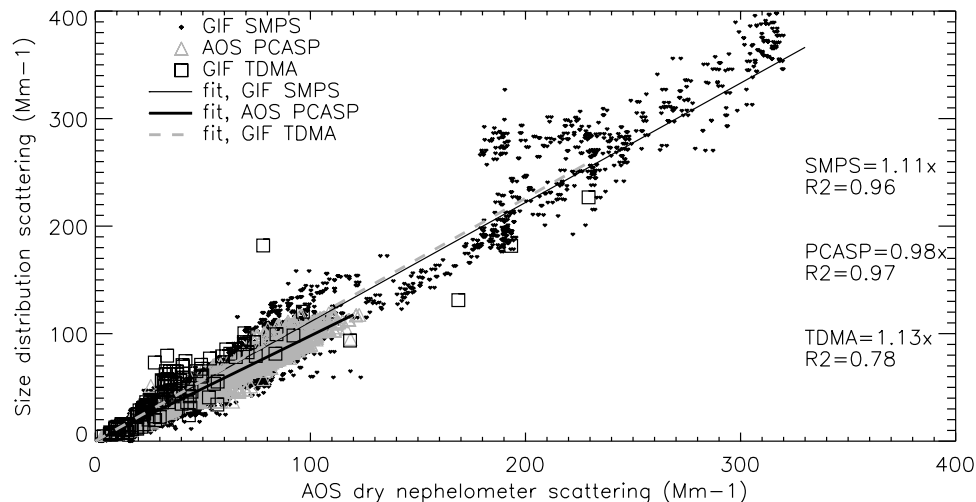
Figure 1. Calculated submicrometer scattering derived from various size distribution instruments (GIF SMPS, AOS PCASP, and GIF TDMA), assuming RI = 1.55 + 0.015i compared with scattering measured by AOS nephelometer for low-RH conditions.

achieved was much lower, around 75%. Particles exiting the first nephelometer are exposed to the scanned humidities and enter the second nephelometer. Fits to the data from these humidity scans can be used to predict the value of light scattering at ambient humidity conditions. Here the dry nephelometer measurements were adjusted to ambient RH conditions using the average fit parameters a and b for the "2-parameter" fit [*Sheridan et al.*, 2001] over the course of the IOP:

$$\sigma(RH\%) = \sigma(40\%) * a * [1 - (RH\%/100)]^{-b} \qquad (2)$$

where σ is either σ_{sp} or σ_{bsp} and RH% is the measured ambient percent relative humidity from the ARM data archive. Scatterplots of nephelometer measured wet σ_{sp} and σ_{bsp} versus the wet σ_{sp} and σ_{bsp} calculated from dry nephelometer measurements and equation (2) showed excellent agreement (slopes = 1.05 and 1.00 respectively, R^2 = 0.99 for both). This agreement gives us confidence in our adjustment of nephelometer measurements to ambient relative humidity conditions. IOP and long-term values for the fit parameters in equation (2) and for f(RH) are given in Table 2. The median value of f(RH) for the IOP is 1.43 which is lower than the long-term median value of 1.68 at the site (on the basis of continuous humidograph measurements between 2000 and 2004). These f(RH) fall in the middle of values reported for other types of aerosol (some examples include the work of *Kotchenruther and Hobbs* [1998] which reported a value of 1.16 for biomass burning smoke in Brazil, while *Sheridan et al.* [2002] reported a values over the Indian Ocean of 2.07 for clean marine aerosol and range of 1.5–1.7 for polluted aerosol).

[20] During the IOP, an optical particle counter (Climet Cl-550, Redlands, California; diameter range 0.35–11.4 μm), a tandem differential mobility analyzer (TDMA; diameter range 0.01–1.0 μm) and a scanning mobility particle sizer (SMPS; column: TSI#3081, CPC: TSI#3010; diameter range 0.03–0.82 μm) were deployed in the GIF trailer to obtain aerosol size distributions. Hereinafter these instruments will be referred to as GIF Climet, GIF TDMA

and GIF SMPS, respectively. For the GIF Climet, the bin diameters are based on the factory calibration using particles with RI = 1.58. For low–relative humidity conditions, comparison of the submicrometer scattering calculated from the measured size distribution from the GIF Climet instrument (assuming RI = 1.55 + 0.015i and λ = 550 nm) showed good correlation (R^2 = 0.93) with the AOS nephelometer submicrometer scattering, however the submicrometer scattering calculated from the GIF Climet tended to be about 25% lower than that measured by the AOS nephelometer. This is due to significant scattering contribution from particles in the 0.1–0.35 μm size range not measured by the GIF Climet. The manufacturer reports an uncertainty of 2% for particle diameter and 10% for particle counts.

[21] For low–relative humidity conditions, comparison of the scattering calculated from the measured size distribution from the GIF TDMA and the GIF SMPS instruments (also assuming RI = 1.55 + 0.015i and λ = 550 nm) showed good agreement (within 11% with R^2 = 0.96 for the SMPS, and within 13% with R^2 = 0.78 for the GIF TDMA) with the measured submicrometer scattering. From 4 to 19 May the GIF TDMA measured size distributions in the range 0.01–0.75 μm mobility diameter, while from 19 May until the end of study, the GIF TDMA measured diameters up to 1 μm. There is no noticeable change in the scattering comparison after 19 May when the larger particles are included in the GIF TDMA data analysis. More details about the GIF TDMA data during the IOP are presented by *Gasparini et al.* [2006], while J. Wang et al. (Aerosol size distributions

Table 2. Average Nephelometer Humidity Scan Fit Parameters for Equation (2), Both for IOP and for All 4 Years (2000–2003) of SGP Humidified Nephelometer Data for sub-μm Data for Wavelength = 550 nm[a]

Parameter	a_iop	b_iop	a_all	b_all
Scattering (λ = 550 nm)	0.93	0.29	0.84 (0.10)	0.37 (0.15)
Backscattering (λ = 550 nm)	1.02	0.10	0.96 (0.16)	0.12 (0.15)

[a]Standard deviations for the long-term fits are in parentheses.

during ARM aerosol IOP, submitted to *Journal of Geophysical Research*, 2005) present an analysis of the GIF SMPS data. The GIF SMPS was calibrated using polystyrene latex spheres of standard sizes. The uncertainty in size measurement is less than 3%, and the uncertainty in concentration measurement is about 10%. *Wang et al.* [2002] present a careful analysis of the uncertainty of their SMPS measurements for the ACE-Asia field campaign; they note that the concentration and size measurements are the most important source of uncertainty in calculating extinction from size distribution measurements and may have contributed up to ±30% uncertainty in the calculated extinction during the ACE-Asia study.

[22] In addition to aerosol size distributions, the GIF TDMA also measured size-resolved hygroscopic growth for a subset of diameters. The combination of these measurements can be used to derive a compositionally resolved size distribution consisting of four solubility categories: soluble, mixed soluble, mixed insoluble, and insoluble [*Gasparini et al.*, 2004]. Each solubility category is assigned a representative refractive index and the optical properties are calculated on the basis of the size- and solubility-resolved concentration of particles. We will use this GIF TDMA inferred composition to investigate the sensitivity of the asymmetry factor to aerosol composition.

[23] The Aerosol Robotic Network (AERONET) Cimel Sun/sky scanning radiometer is located at the surface near the AOS and GIF trailers. The basic AERONET data product is spectral aerosol optical depth in the wavelength range (340–1020 nm). Other data products such as column-averaged aerosol size distributions and asymmetry parameters are derived for four wavelengths (440, 670, 870, and 1020 nm) using Dubovik's algorithm [*Dubovik and King*, 2000] and are available on the AERONET website. Here level 2.0, cloud-screened data were used. The minimum AOD for the Dubovik retrievals to work is 0.4 at 440 nm. Uncertainties in the retrieval of asymmetry parameter from AERONET data are in the range 3–5%; these small uncertainties reflect the fact that g is an integral characteristic of the aerosol (A. Smirnov, personal communication, 2005).

2.2. Airborne Aerosol Instrumentation

[24] During the IOP, two aircraft with aerosol optical and microphysical instrumentation flew various flight tracks over the site in order to make measurements of aerosol properties aloft. One airplane was the in situ aerosol profiling (IAP) Cessna, which has been making routine profile flights to measure aerosol optical properties over SGP since 2000 (over 530 flights as of December 2004). The second airplane was the Center for Interdisciplinary Remotely Piloted Aircraft Studies (CIRPAS) Twin Otter (TO) which was deployed specifically for the IOP.

[25] The IAP program routinely (2–3 times per week) measures aerosol optical property profiles over SGP using a small airplane (Cessna 172-N). The aerosol package on the airplane is similar to that in the AOS trailer (i.e., nephelometer, PSAP at low RH) and is described in more detail by *Andrews et al.* [2004]. There is a 1 μm impactor upstream of the aerosol instruments (corresponding to a geometric size cut of approximately 0.79 μm) on the Cessna to eliminate uncertainties due to particle losses and inlet

transmission inefficiency for larger particles. During the IOP the Cessna flew 14 of its standard profile flights. The uncertainties in the nephelometer measurements for the IAP airplane depend primarily on the flight segment length (~10 min for the four highest levels, ~5 min for the five lowest levels) and on the amount of aerosol present [*Clarke et al.*, 2002]. For very clean ($\sigma_{sp} \sim 1$ Mm^{-1}) upper flight levels the uncertainty in the scattering measurement is approximately 40%, while for flight levels with more aerosol ($\sigma_{sp} > 20$ Mm^{-1}) the uncertainty will be less than 10%.

[26] The Twin Otter (TO) can carry a much larger payload than the Cessna and as such had a larger suite of measurements [e.g., *Schmid et al.*, 2004; A. W. Strawa et al., In situ measurement of aerosol optical properties made during the DOE Aerosol IOP: 1. Comparison of extinction and scattering coefficients, submitted to *Journal of Geophysical Research*, 2005, hereinafter referred to as Strawa et al., submitted manuscript, 2005]. The instrumentation on board the TO included a humidograph system consisting of three Radiance Research nephelometers (Model M903), TSI nephelometer, 3-wavelength PSAP, PCASP, SMPS, and the AATS-14 sunphotometer (Table 1). The Twin Otter instrumentation will be preceded by TO to differentiate it from similar instruments on the IAP aircraft and at the surface. The TO did not have an impactor or other size cut device on its sampling inlet and thus was not limited to sampling submicrometer aerosol. The TO flew 17 flights during the IOP, five of which were side-by-side profile flights with the IAP aircraft.

[27] As mentioned above, during the IOP the IAP aircraft continued to fly its normal flight profiles and the Twin Otter occasionally flew a profile side-by-side with the Cessna as part of longer flight tracks. For the comparison purposes here, we focus on the five side-by-side profile flights flown by the two aircraft on 7, 9, 17, 25 and 29 May. For each side-by-side profile flight, the Cessna flew nine level legs over (or near) the surface site. The legs were flown at altitudes of 467, 610, 915, 1220, 1525, 1830, 2440, 3050, 3660 m asl (these altitudes correspond to flight levels of 1500, 2000, 3000, 4000, 5000, 6000, 8000, 10000 and 12000 feet). The Twin Otter did not fly the lowest flight level side-by-side with the IAP Cessna because of safety constraints. Three of the side-by-side flights contained the maximum possible eight legs for comparison (7, 9, and 17 May), unfortunately in one of those flights (17 May) the IAP plane recorded data at 1 min resolution, which limits its value for comparison. The other two flights (25 and 29 May) had seven and two side-by-side legs respectively.

[28] Comparisons of low-RH, light scattering measurements by TSI nephelometers aboard the two airplanes during side-by-side flight legs showed the observations were correlated (R^2 between 0.60 and 0.97 for the three flights with seven or more side-by-side legs), with the ratio of σ_{sp}(IAP)/σ_{sp}(TO) ranging from 0.6 to 1.1. Some of the observed differences between the two airplanes are due to differences in the sample inlet size cut for the two airplanes; better agreement was found between the two platforms when the aerosol Ångström exponent was large, indicating the predominance of submicrometer particles (Strawa et al., submitted manuscript, 2005). Overall uncertainties in the TO TSI nephelometer measurements will be slightly higher than those for the IAP nephelometer because it is measuring

supermicron as well as submicron aerosol. A detailed discussion of uncertainty issues for a previous deployment of the in situ aerosol optical system on the Twin Otter is provided by *Anderson et al.* [2003].

[29] The TO SMPS [*Wang et al.*, 2003] measured dry aerosol size distributions in the range 0.02–0.73 μm. Humidity in the TO SMPS was always less than 30%. On the basis of segment averages, the calculated scattering from the TO SMPS is approximately 85% of the submicrometer scattering measured on the IAP airplane but the values were well correlated (R^2 = 0.93). Some of the difference between the two scattering values may be due to the difference in inlet size cut for the TO SMPS and IAP nephelometer. The uncertainty for the TO SMPS is as described for the GIF SMPS.

[30] The TO PCASP (PMS Inc., Boulder, Colorado) with a SPP-200 data system (DMT Inc., Boulder, Colorado) measured particles in the size range 0.11–2.69 μm. The data from the TO PCASP are reported at ambient temperature and pressure conditions but low RH. Scattering calculated from the TO PCASP is significantly lower (34%) than the submicrometer scattering measured by the IAP nephelometer, but again the correlation between measured and calculated scattering is excellent (R^2 = 0.96). TO PCASP-derived scattering is also much lower than that measured by the TO nephelometer. The Twin Otter PCASP was calibrated using spheres of three different refractive indices (1.33, 1.42 and 1.58) using the methodology described by *Liu et al.* [1992]. The bin diameters used in this study were based on the RI = 1.58 calibration. On the basis of the calibrations, there is a 20–30% shift in diameter for the TO PCASP between RI = 1.33 and RI = 1.58. Previous deployments of this instrument report uncertainties in the size range measurements of ±6% [*Hegg and Jonsson*, 2000].

[31] The Ames airborne tracking 14-channel sunphotometer (AATS-14) was deployed on the Twin Otter to measure aerosol optical depth and spectral extinction in the range 354–2139 nm [*Schmid et al.*, 2006]. *Schmid et al.* [2006] found the TO AATS-14 measurements during the IOP to be well correlated with the in situ instruments aboard the Twin Otter (R^2 > 0.8), but the AATS AOD was 18% higher (at 519 nm) than the AOD estimated from TO nephelometer and PSAP instruments. They note that possible explanations for the lower in situ AOD include: losses of large particles due to inlet effects, uncertainties in humidity correction, change in particle size due to evaporation of volatile materials other than water and issues with filter-based measurements (i.e., PSAP). Here, because we are just looking at side-by-side TO and IAP data, we look at how AATS derived and measured scattering compare for the level flight legs. The King inversion routine [*King et al.*, 1978] was used to process the TO AATS-14 spectral aerosol optical depth measurements (see next section for details) and derive aerosol size distributions. Although the King inversion was able to reproduce the input TO AATS-14 spectral AOD measurements within 5% over a wide range of AOD conditions (0.05 < AOD < 0.35 at 519 nm), the light scattering values calculated from the derived size distributions were often significantly different (factor of 3) than the scattering measured by the TO nephelometer. This is likely due to differences in vertical resolution; *Schmid et*

al. [2006] used smooth continuous ascents or descents in their comparisons allowing for much higher vertical resolution of the aerosol profile, while here the relatively coarse side-by-side flight levels (separated by 300–600 m) were used. If the aerosol is not vertically homogeneous from one flight level to the next, the comparison with in situ measurements may not be in good agreement. Looking at the ambient scattering values for the descents between flight levels for the TO nephelometer suggests that there is indeed vertical inhomogeneity between levels. Whether these differences in scattering between the in situ and remote instruments correspond with differences in asymmetry parameter will be discussed in the results section. The uncertainty in the spectral AOD measurements ranged from approximately 0.002 to 0.02, depending on wavelength and flight. More discussion of the uncertainty in the TO AATS-14 AOD measurements are given by *Schmid et al.* [2006, and references therein].

[32] In general, comparison of measured and calculated scattering showed these values were well correlated among the different platforms, R^2 > 0.9, with the exception of the GIF TDMA (R^2 = 0.78) and AATS-14 (R^2 = 0.8, based on *Schmid et al.* [2004]). The actual values of the scattering intercomparisons did not suggest quite as good agreement. However, for deriving *g*, the correlation rather than the absolute value of scattering is the critical factor because *g* is an intensive parameter [*Ogren*, 1995] and thus is independent of the absolute amount of aerosol present. As we show in the following section it is the size distribution (size and width) and wavelength which are the most important factors for determining *g*.

2.3. Methods for Deriving *g* From Various Aerosol Measurements

[33] The information needed to calculate *g* on the basis of aerosol physical properties includes the aerosol size distribution, refractive index and particle shape. With these data in hand, Mie theory (in the case of spherical particles) or discrete dipole approximation (DDA) or T-matrix calculations (for nonspherical particles) can be used to calculate the aerosol optical properties. Size distributions can be measured directly with in situ aerosol size instrumentation, but another way to obtain a size distribution is the inversion of spectral aerosol optical depth or light extinction measurements [e.g., *King et al.*, 1978; *Fiebig et al.*, 2005]. Refractive index values can be estimated from aerosol chemistry and/or size-resolved hygroscopicity (e.g., R. Gasparini et al., Comparison of humidity-dependent optical properties and CCN spectra derived using size-resolved hygroscopicity with direct measurements made at the ARM Southern Great Plains site, submitted to *Journal of Geophysical Research,* 2005, hereinafter referred to as Gasparini et al., submitted manuscript, 2005) measurements. In the case of chemical measurements, the low time resolution and limited number of species analyzed often make this method no better than assuming a reasonable value for the refractive index. As is shown later, assuming a reasonable refractive index for dry aerosol does not have a significant effect (less than 3%) on the calculated light scattering. At ambient humidities, the change in refractive index and particle size due to water uptake can be significant and will influence the calculated optical properties. *Hartley and Hobbs* [2001], for

example, show the strong influence of RH on g, where g increases with RH.

[34] For the aerosol size distribution measurements made during the IOP (and for size distributions derived from spectral AOD or scattering measurements), homogeneous, spherical particles are assumed, and Mie theory is used to calculate an asymmetry parameter at 550 nm. This provides for convenient comparison to the nephelometer-derived g at 550 nm. A refractive index of $1.55 + 0.015i$ is assumed for measurements made below 40% RH. This value results in good agreement between measured and calculated scattering as noted in the instrument descriptions. To go from an asymmetry parameter for a single particle to an asymmetry parameter representing the aerosol size distribution the following equation [d'Almeida et al., 1991] is used:

$$g = \frac{\sum_i g_i \sigma_{sp,i}}{\sum_i \sigma_{sp,i}} \quad (3)$$

where i indicates the aerosol size bin.

[35] If both σ_{sp} and σ_{bsp} are measured then the backscattering fraction b can be calculated. Here the backscatter fraction (b) refers to the ratio of light scattered into the backward hemisphere (backscatter, σ_{bsp})) to total light scattering (σ_{sp}) measured by the nephelometer. With b an alternative approach for deriving asymmetry parameter applying the Henyey-Greenstein approximation [e.g., Wiscombe and Grams, 1976] can be used. Wiscombe and Grams [1976] plot a smooth relationship between b (which they call $\beta(1)$) and g in their Figure 3. The fit equation based on that plot relating b to g is (P. Arnott, personal communication, 2002):

$$g = -7.143889*b^3 + 7.464439*b^2 - 3.96356*b + 0.9893 \quad (4)$$

Marshall et al. [1995] suggest a more complex relationship between b and g which depends on the imaginary part of the refractive index and the width of the aerosol size distribution.

[36] A new data inversion technique [Fiebig et al., 2005] is also applied to derive the asymmetry parameter from the low-humidity AOS and IAP aerosol system measurements (aerosol light absorption and spectral light scattering and backscattering). The 1 and 10 μm impactors upstream of the nephelometer provide geometric aerosol size cuts of 0.79 and 7.9 μm respectively, which allows for separation of the aerosol into fine (dp < 0.79 μm) and coarse (0.79 μm < dp < 7.9 μm) size modes. The particles are represented by homogenous, internally mixed spheres composed of ammonium sulfate, soot and water over the entire size range. (Note: not including organic aerosol as one of the components is unlikely to affect the inversion results for dry aerosol as the organics can be assumed to have similar RI as ammonium sulfate.) The aerosol chemical composition is parameterized by a soot volume fraction f_{soot} and a water volume fraction f_{H2O} for the absorbing and nonabsorbing portions of the aerosol. The algorithm does not assume an initial guess for the aerosol size distribution, rather it requires knowledge of the instrument transfer function, i.e., what fraction of particles of each size are sensed by

the instrument. During the inversion, the PSAP and nephelometer (including angular truncation effects) responses are calculated for each size mode. The measured particle scattering coefficients are used to derive a particle size distribution and the inversion algorithm discretizes the particle size distribution into logarithmic equidistant bins. In an iterative process, the values for f_{soot} and f_{H2O} are varied so that the measured light absorption and backscattering coefficients, respectively, are reproduced by the inversion result. Iterations are done first for the fine mode and then for the coarse mode. For an inversion to be deemed successful, the calculated responses must match the measurements. The inversion's final output is an aerosol size distribution and chemical composition from which refractive index can be determined and thus the asymmetry parameter can be calculated using Mie theory. The median RI retrieved for the IOP aerosol was $1.55 + 0.015i$. The inversion does not retrieve information about the state of mixture of the soot component, the soot size distribution and the particle density and this results in a systematic uncertainty in the retrieved asymmetry parameter of approximately 1% at 550 nm in both size ranges (M. Fiebig and J. A. Ogren, Retrieval and climatology of the aerosol asymmetry parameter at the CMDL aerosol baseline stations, submitted to Journal of Geophysical Research, 2005). For the surface and airborne CMDL measurements, we will use both equation (4) and the Fiebig inversion scheme to derive values for asymmetry parameters.

[37] For the remote sensing instruments (AERONET and TO AATS-14) different data inversion techniques are employed to derive an asymmetry parameter. For the AERONET measurements, the data inversion algorithm [Dubovik and King, 2000; Dubovik et al., 2000] assumes that the particles are homogenous spheres, although the composition (i.e., index of refraction) is not fixed. Both of these remote sensing instruments make measurements at ambient conditions so that no relative humidity adjustment is needed.

[38] For the TO AATS-14 data, the inversion algorithm by King et al. [1978] is used to calculate aerosol size distributions consistent with the measured optical depths. The basic requirements of the inversion are spectral AOD and their associated uncertainties, an assumed refractive index, and diameter limits for the size distribution. It is up to the user to choose which of the many aerosol size distributions output by the inversion algorithm is most representative of the actual aerosol. King [1982] shows successful application of the inversion for $0.01 < AOD < 2.0$. The measurements of in situ size distributions and aerosol optical properties made on the Twin Otter simultaneous with the TO AATS-14 observations are used here to constrain the choice of size distribution. The King algorithm assumes spherical, homogenous particles and a constant refractive index over the entire size range, the same assumptions used in the Mie theory calculations. Because the input data to the inversion algorithm is aerosol optical depth the result is a "columnar" aerosol size distribution, i.e., "number of particles per unit area per unit log radius interval in a vertical column in the atmosphere" and has units of cm^{-2}. To correctly compare asymmetry parameters derived from the TO AATS-14 with those derived from in situ instruments during a flight leg two things must be done.

Table 3. Summary of Calculated Asymmetry Parameters (dp < 1 μm Unless Otherwise Noted)[a]

Instrument	g Range (STP, Dry)	g Median (STP, Dry)	g Range (Ambient)	g Median (Ambient)
AOS nephelometer				
Equation (4)	0.49–0.67	0.59	0.51–0.80	0.65
Fiebig dp < 0.79 μm	0.47–0.61	0.55	n/a	n/a
Fiebig dp < 7.9 μm	0.51–0.67	0.58	n/a	n/a
AOS PCASP				
dp < 1 μm	0.59–0.67	0.63	n/a	n/a
dp < 10 μm	0.61–0.65	0.65	n/a	n/a
GIF Climet	0.66–0.69	0.67	n/a	n/a
GIF TDMA	0.57–0.66	0.63	0.67–0.75[b]	0.69
GIF SMPS	0.52–0.65	0.60	n/a	n/a
IAP nephelometer	0.35–0.72	0.59	0.51–0.71[b]	0.61
IAP nephelometer	0.48–0.69[c]	0.61	n/a	n/a
TO nephelometer[c,d]	0.51–0.65	0.59	0.52–0.67	0.60
TO SMPS[c]	0.57–0.68	0.61	n/a	n/a
TO PCASP[c]	0.46–0.62	0.55	n/a	n/a
TO AATS[c,d]	n/a	n/a	0.63–0.76	0.72
AERONET[d,e]	n/a	n/a	0.69–0.71	0.70

[a]Range is 5th and 95th percentile.
[b]RI = 1.40+0.015i, growth rate = 1.45.
[c]Based on g for flight legs (not column average).
[d]No size cut.
[e]Column value. (Note that not all instruments were operational/invertible for all flight levels.)

First, the AOD contribution from each flight leg must be determined. Because the TO AATS-14 measures AOD in the atmospheric column between the aircraft and the top of the atmosphere, this calculation is straightforward: $AOD_{\Delta i} = AOD_i - AOD_{i+1}$ where i is the level of interest and i + 1 is the level above it. Second, the size distribution resulting from the inversion must be divided by the assumed vertical thickness of the flight leg (Δ_i), i.e., the portion of the column over which AOD was calculated, e.g., $\Delta_i = z_{i+1} - z_i$. Here z_i is the altitude of the level of interest and z_{i+1} is the altitude of the level above it. This division gives the calculated number concentration in units of cm^{-3} and thus should make the number concentration comparable to other size distributions and also can be directly input into Mie scattering code.

[39] The King inversion can be used to derive a value for g [*Gonzalez-Jorge and Ogren*, 1996] for the total column at ambient conditions by using the TO AATS-14 measurements for the lowest flight leg. Likewise, the AERONET g is a column value at ambient conditions. Calculating g for the total column for the in situ airborne instruments first requires calculation of g for the individual flight layers weighted by the scattering coefficient and then summing over the flight levels normalized by level thickness Δ_i and scattering coefficient:

$$g_{col} = \Sigma\Delta_i\,g_i\,\sigma_{sp,i}/\Sigma\Delta_i\,\sigma_{sp,i} \tag{5}$$

We will do this for all of the profile flights over SGP during the IOP: all the IAP flights during the IOP and the three TO flights (DOY 127, 129 and 145) that were side-by-side with IAP plane for seven or more flight levels for both ambient and low-RH conditions.

3. Results

[40] Here we first present results showing how the different estimates of asymmetry parameter compare and then discuss how these findings influence our understanding of asymmetry parameter and, consequently, radiative forc-

ing. Table 3 summarizes the values of asymmetry parameter found for the different instruments and platforms during the IOP. The range of median g values at ambient conditions found during the IOP ($0.60 < g < 0.72$) are in the range of values for g reported for other experimental studies. *Hartley and Hobbs* [2001] reported a median value of 0.7 for aerosol measured during the TARFOX campaign off the East Coast of the United States, while *Eck et al.* [2001] found the same value for polluted aerosol observed during the Indian Ocean Experiment (INDOEX). *Formenti et al.* [2000] found slightly higher values (0.72–0.73) for Saharan dust aerosol. measured during the ACE-2 program. Significantly lower values have been reported for smoke aerosol: *Ross et al.* [1998] found g values of approximately 0.54 for biomass burning in Brazil, while *Wong and Li* [2002] suggested values as low as 0.4 might be possible on the basis of satellite retrievals for boreal forest fire events.

3.1. Comparison of Surface Measurement-Derived Asymmetry Parameters

[41] At the surface, the average ratios of dry (RH < 40%) asymmetry parameter calculated from nephelometer measurements using equation (4) to the dry asymmetry parameter calculated from measured size distributions (AOS PCASP, GIF SMPS, GIF TDMA) are 0.97 ± 0.05, 1.00 ± 0.07 and 0.94 ± 0.05, respectively, and the range of g for all instruments is quite similar. Figure 2a shows g from the nephelometer (and equation (4)) and from the AOS PCASP at low-RH conditions. They track each other quite well. The asymmetry parameter derived from GIF Climet size distribution measurements is significantly higher than the other ground-based in situ measurements. This is due to the GIF Climet instrument not sensing particles with diameters less than 0.35 μm; using the GIF SMPS size distribution data just in the submicrometer size range measured by the GIF Climet (e.g., between 0.35 and 1 μm) also results in a median value for g of 0.67. The AERONET retrieval of column-averaged asymmetry parameter is larger than the dry surface values for g calculated using the various aerosol size distribution instruments and the nephelometer, however
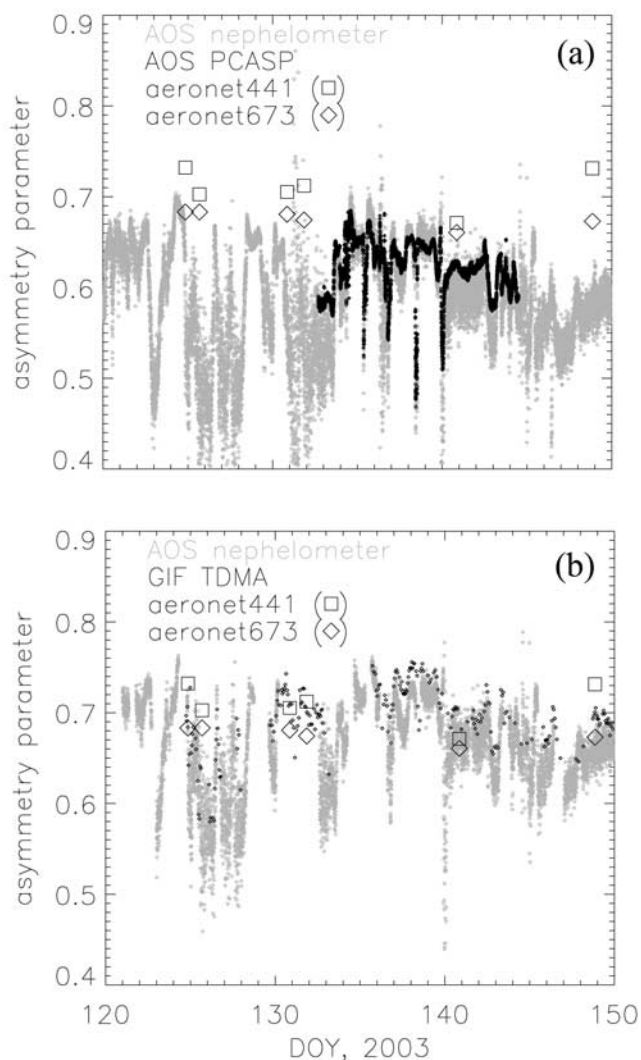
Figure 2. Time series comparison of asymmetry parameter for $\lambda = 550$ nm (a) dry AOS nephelometer and AOS PCASP with AERONET (ambient) and (b) AOS nephelometer (adjusted to ambient RH) and GIF TDMA (at 85% RH) with AERONET (ambient).

the AERONET value is for the whole column and for ambient RH. Plots comparable to Figure 2a could be made for the other size distribution instruments (GIF SMPS, GIF TDMA) as well.

[42] Figure 2b shows the g derived from AOS nephelometer measurements adjusted to ambient conditions along with GIF TDMA measurements at 85% RH. The AOS nephelometer measurements were adjusted to ambient conditions using SGP meteorology data from the ARM web site and the average f(RH) fit data for the IOP. This adjustment to more realistic relative humidity conditions shifts the calculated AOS nephelometer asymmetry values at the surface closer to those derived from the AERONET measurements. Since the atmosphere was typically more humid than the reference conditions (RH < 40%) measured by the low-humidity AOS nephelometer, this shows that composition, in particular as it affects aerosol hygroscopic growth, can play an important role in determining the asymmetry

parameter of atmospheric aerosol. This is consistent with *Hartley and Hobbs* [2001] and *d'Almeida et al.* [1991] observations that higher humidity conditions lead to higher asymmetry parameter values.

[43] Asymmetry parameters were also calculated for the AOS nephelometer using the new inversion scheme developed by *Fiebig et al.* [2005]. For the total aerosol (dp < 7.9 μm), the Fiebig values generally correlated quite well with the values calculated from equation (4) ($R^2 = 0.88$) and the average ratio of g(Eq4)/g(Fie) was 0.94 ± 0.04. The Fiebig values were typically higher than the values derived using equation (4). The agreement between the two methods was lowest when the submicrometer fraction of aerosol ($R_{sp} = \sigma_{sp}(dp < 1 \, \mu m)/\sigma_{sp}(dp < 10 \, \mu m)$) was lowest: i.e., when more coarse aerosol was present. For $R_{sp} > 0.7$ the two methods were within 10%, while $R_{sp} < 0.7$ the ratio decreased rapidly with increasing amounts of coarse aerosol. Even for low R_{sp}, however, the two methods were within 20%. For comparison based only on the submicrometer nephelometer data, the average value of the ratio g(Eq4)/g(Fie) was 1.0 ± 0.04 and the correlation was ($R^2 = 0.90$). This increased agreement for the submicrometer aerosol is consistent with the observation that higher values of Rsp corresponded to better agreement between the two methods. The relationship between the size distribution-derived g and the Fiebig g was very similar to that of the size distribution-derived g and the nephelometer submicrometer g derived from equation (4).

3.2. Comparison of Airborne Measurement-Derived Asymmetry Parameters

[44] Similar to the surface measurements, the median calculated asymmetry parameter from the TO SMPS size distributions agreed quite well with that calculated from equation (4) and the IAP nephelometer (Figure 3). Data from the TO PCASP exhibit quite different behavior than the other size distribution-based measurements. As noted before, the submicrometer scattering calculated from the TO PCASP was only about 66% of that measured by the IAP nephelometer. The median asymmetry parameter from the TO PCASP is lower than the TO and IAP nephelometer-based measurements and is in fact the lowest asymmetry
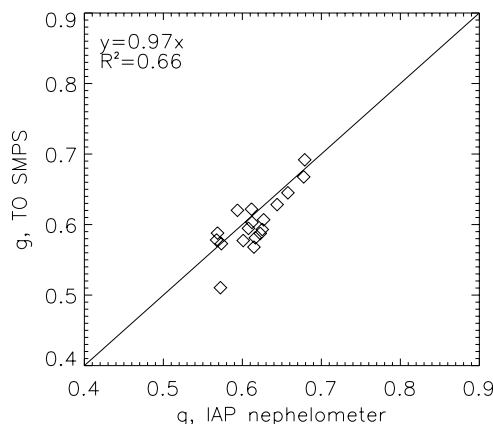

Figure 3. Plot of segment average values of asymmetry parameter for dry conditions at $\lambda = 550$ nm for the IAP nephelometer and the TO SMPS.
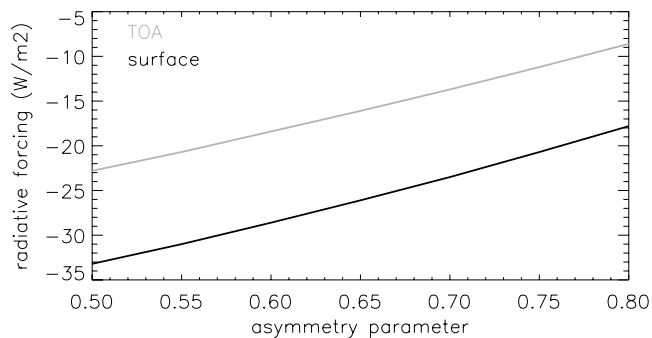
Figure 4. Change in TOA and surface radiative forcing calculated using SBDART as a function of g.

parameter for any of the instruments. Put together, these observations suggest that the TO PCASP may be missing some fraction of particles.

[45] Because of the plethora of size distributions produced by the King inversion, all of which reproduce the AOD measured by the TO AATS-14, both the potential variation in g due to these different size distributions as well as the overall variation in g for the flights studied can be discussed. For most flight levels the different size distributions resulted in the derived g values within 1% of the median value for that flight. For very clean flight levels (AOD values less than 0.007 at visible wavelengths) there was more variability (±5% of median value). This is likely because the measured AOD values were within the uncertainty range for AOD. Flight level asymmetry parameters calculated from the TO AATS-14 and from the TO nephelometer measurements at ambient conditions were poorly correlated, suggesting that the AATS was probably detecting different aerosol than the in situ nephelometer because of vertical inhomogeneity. In general, larger values of g were more often associated with the TO AATS-14 than with the ambient TO nephelometer measurements, consistent with the idea that the TO AATS-14 measures all ambient aerosol, while the in situ instruments may have some losses of large particles during sampling.

4. Discussion

[46] The results show that the values of asymmetry parameter calculated from different measurement techniques and platforms are quite similar (i.e., Table 3). Here we discuss the implications that the observed range in g has on radiative forcing and what we can learn from our approach about the factors that influence g at the SGP site. We do this by specifically addressing each of the scientific questions listed in the introduction.

4.1. What is the Range of Values for g at This Site? How Does This Range Affect Calculations of Aerosol Forcing?

[47] Here we use the range of derived values of the asymmetry parameter from a variety of platforms and instruments to assess the sensitivity of estimates of aerosol forcing to values of asymmetry parameter. Using a radiative transfer model (SBDART [*Ricchiazzi et al.*, 1998]) and IOP median values of ambient AOD (0.08) and single scattering albedo, ω_o, (0.95 calculated from the AOS nephelometer

and PSAP, $\omega_o = \sigma_{sp}/(\sigma_{sp} + \sigma_{ap})$), the values for aerosol forcing at the surface and top of atmosphere were calculated for the range of g (0.5–0.8) observed during the IOP for $\lambda = 550$ nm. At the surface, the forcing for the median g (0.65 at ambient conditions) was −26.1 W m^{-2}, while TOA forcing was −16.1 W m^{-2}. An assumed 10% decrease in g resulted in a 19% reduction in TOA forcing, similar to the 12% value determined by *Marshall et al.* [1995], while the surface forcing decreased by 13% for the same reduction in g. Figure 4 shows the change in surface and TOA forcing caused by perturbing the ambient asymmetry parameter over the range of asymmetry parameter values seen during the IOP while holding all other input parameters constant. A physical interpretation of Figure 4 is that as the asymmetry parameter increases toward its maximum value of 1 (i.e., totally forward scattered light) there is less scattering of incoming radiation back to its source and thus there is less of an aerosol forcing effect both at the surface and TOA.

[48] Because b is the value directly calculated from nephelometer measurements, and because many other in situ aerosol measurements have been analyzed using the formulation of *Haywood and Shine* [1995, equation 3], a similar exercise can be performed for radiative forcing efficiency (RFE = $\Delta F/\delta_o$) where ΔF is the top of atmosphere aerosol forcing and δ_o is the "unit" aerosol optical depth 0.01. The assumptions for this calculation are listed in Table 4. We did two types of RFE calculations. In the first, ω_o at low-RH conditions was held constant at the May 2003 median value (0.92 calculated from the AOS nephelometer and PSAP) while b was varied over the range observed during the study (0.09 < b < 0.17). This resulted in values of RFE between −21 and −30 W/m^2 for $b = 0.09$ and $b = 0.17$ respectively, with a midpoint value of −25 W/m^2 using the median value of $b = 0.13$. In a second, more realistic type of RFE calculation we took into account the systematic variation of b with ω_o observed at SGP (Figure 5a). At low ω_o values, backscatter tends to be high, while there is a continuous decrease in backscatter at the higher end of the ω_o scale. One explanation of the systematic variation of single scattering albedo with backscattering fraction seen in Figure 5a is that wet scavenging of aerosol particles preferentially removes large, hygroscopic particles leaving behind both small particles with high backscattering efficiency as well as absorbing but nonhygroscopic particles such as soot (which are both small and efficient scatterers as well as absorbers), resulting in lower ω_o. The same effect results in the systematic variation of asymmetry parameter with single scattering albedo seen in Figure 5b. For the RFE

Table 4. Parameters Used in Radiative Forcing Efficiency Calculation

Variable	Definition	Value
δ_o	"unit" aerosol optical depth	0.01
ω	aerosol single scattering albedo	varied
β	average aerosol upscatter fraction[a]	varied
D	daylight fraction	0.5
S_o	solar constant	1370 W/m^2
T_{at}	atmospheric transmission	0.76
A_s	cloud fraction	0.6
R_s	surface reflectance	0.15

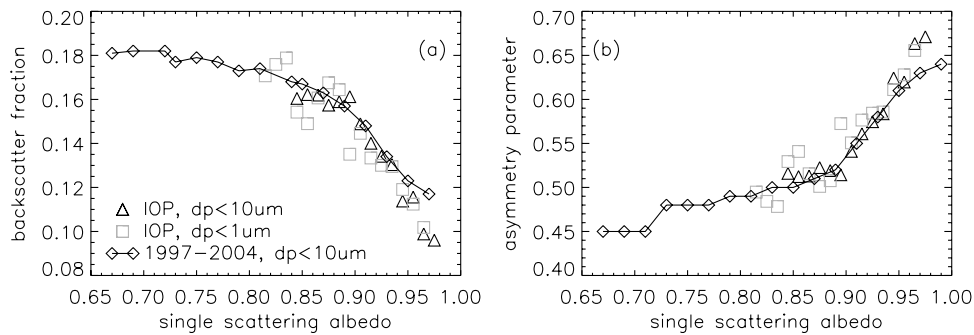[a]$\beta = 0.0817 + 1.8495b − 2.9682b^2$.

Figure 5. Systematic variation at dry conditions, λ = 550 nm of single scattering albedo with (a) backscattering fraction b and (b) asymmetry parameter. Triangles and squares represent May 2003 IOP data, and the line with diamonds represents 8 years of SGP AOS data (1997–2004).

calculations described above, the range of forcing was more limited (-20 < RFE < -26 W/m^2), consistent with the offsetting of contributions from b and ω_o noted by *Delene and Ogren* [2002]. Again the higher value of RFE corresponds to the lower value of b.

[49] While the radiative forcing calculations described above were done for λ = 550 nm, a more complete understanding of aerosol forcing requires considering the spectral dependence of relevant parameters. Asymmetry parameter is one of the variables contributing to the spectral dependence of forcing. Figure 6 shows how g derived from Mie theory applied to the low-RH (RH < 40%) GIF SMPS data decreases with λ. The spectral dependence of g on wavelength is similar to that shown by *Eck et al.* [2001] for aerosol observed over the Indian Ocean, however, they retrieve values for g at ambient conditions and thus present values of g that are about 15% higher than shown in Figure 6. This is consistent with the difference observed in this study for dry and ambient values of g (e.g., Table 2).

4.2. How Much Do the Values of g Vary Depending on the Instruments and Method Used to Derive Them?

[50] As shown in Table 3, there is not a lot of variation in the median value and range of g, regardless of method and instrument with the exception of the GIF Climet. The average value (±standard deviation) of g at dry conditions for the surface instruments and methods is 0.60 ± 0.03 (excluding the GIF Climet). This 5% variation in median asymmetry parameter corresponds to approximately a 5% difference in radiative forcing for the surface and a 7% difference for TOA based on the SBDART calculations discussed in the previous section. For ambient conditions g is 0.65(±0.05); the effects of a 10% variation in the value for g have already been discussed.

[51] Because b is readily measured using a nephelometer with backscatter capability and can be calculated from size distribution measurements, the relationship between backscatter fraction and asymmetry parameter can be investigated (Figure 7). As mentioned in the introduction, the relationship between these two quantities is often used to parameterize g in radiative transfer calculations, e.g., the Henyey-Greenstein approximation. At the surface, the asymmetry parameter determined using measured nephelometer backscatter fraction and the Henyey-Greenstein approximation tends to overestimate asymmetry parameter

by 5–15% compared to the asymmetry parameter determined using Mie theory and measured size distributions (dp < 1 μm) for low values of backscatter fraction (i.e., large particles) (Figures 7a–7c). As backscattering fraction increases (i.e., size distribution shifts to smaller particles) the Mie-derived asymmetry parameter approaches the Henyey-Greenstein value (Figures 7a–7c). For the median value of b observed during the IOP (0.13), the two methods agree to within 1% for submicron aerosol size distributions. The AOS PCASP also measures supermicron particles so Mie theory can be used to calculate the relationship between g and b for a wider size range of atmospheric aerosol. Figure 7a shows that, when supermicron aerosol are included in the Mie calculations, the calculated points tend to lie on the Henyey-Greenstein approximation line. Figure 7d shows the same relationship for the Fiebig inversion algorithm. The submicrometer Fiebig values show similar behavior to those of the measured submicron size distributions, while the Henyey-Greenstein approximation underestimates g as a function of b by about 6% compared to the Fiebig inversion results for the total aerosol (e.g., dp <
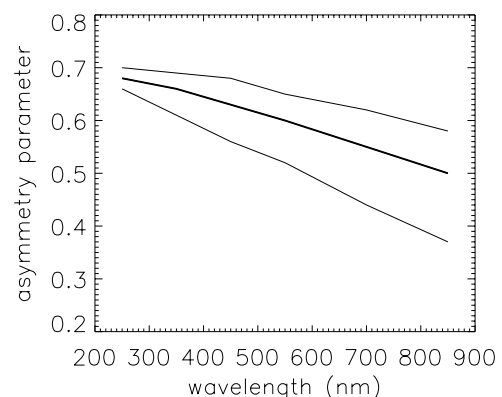

Figure 6. Variation of asymmetry parameter with wavelength for low-RH (RH < 40%) conditions. Values plotted are the median asymmetry parameter (thick line) derived from the GIF SMPS data assuming RI = 1.55 + 0.015i (i.e., no change was made for spectral dependence of RI) and the 5th and 95th percentiles (bottom and top thin lines, respectively).
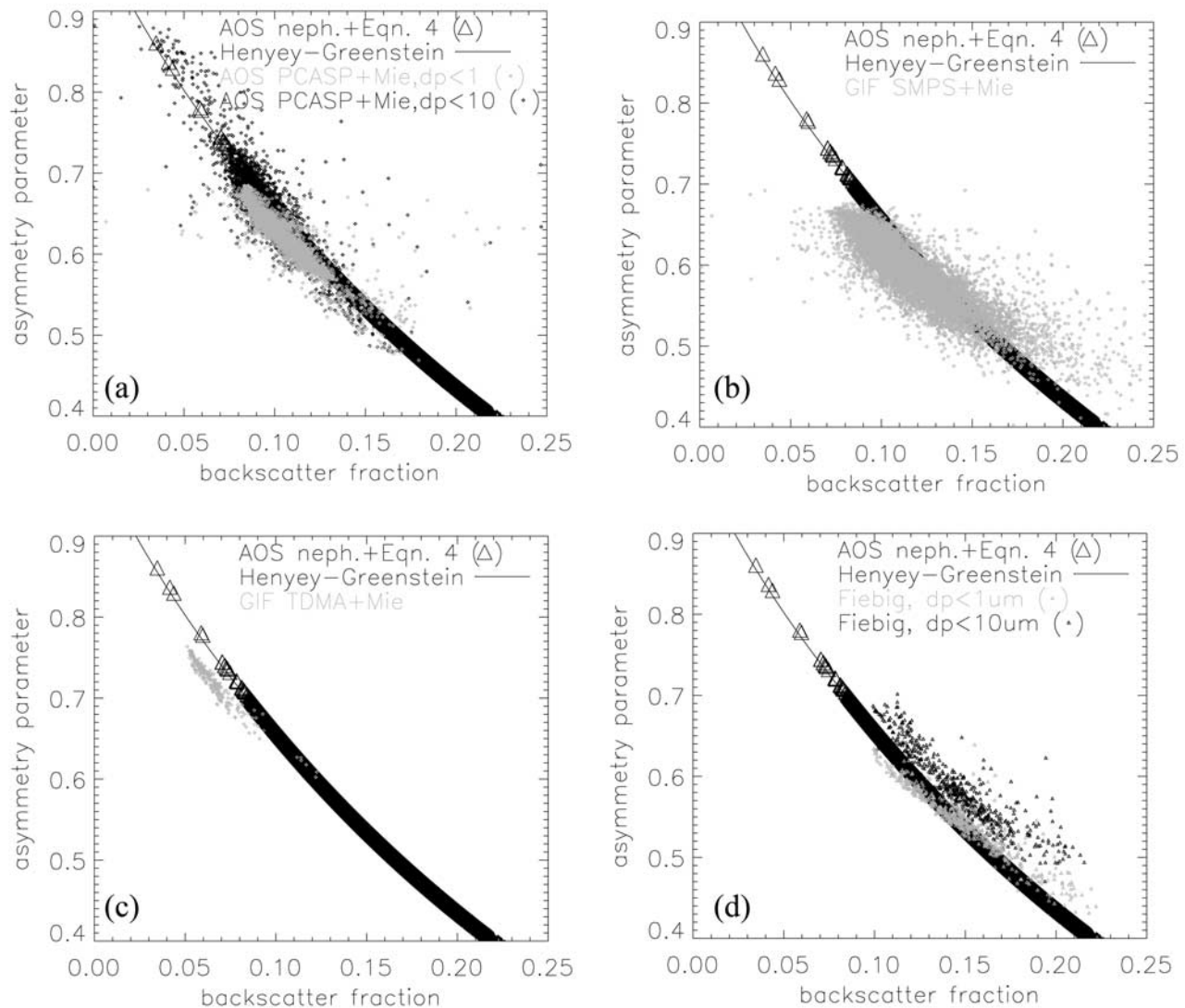
Figure 7. Relationship between backscatter fraction and asymmetry parameter (RH < 40%) (dp < 1 μm except where noted). (a) AOS PCASP, (b) GIF SMPS and (c) GIF TDMA, and (d) Fiebig inversion (low RH conditions, λ = 550 nm, and RI = 1.55 + 0.015i).

7.9 μm). In general, Figure 7 suggests that the Henyey-Greenstein approximation is appropriate both for size distributions consisting of primarily submicron aerosol (e.g., continental, anthropogenic aerosol), based on the Mie calculations for measured submicron size distributions and for size distributions including supermicron aerosol particles (e.g., dust or sea salt) based on the values calculated using the AOS PCASP measurements of particles with dp < 10 μm (Figure 7a).

4.3. Are the Values of *g* Observed at SGP Consistent With Other Indicators of Aerosol Type?

[52] Air mass trajectories are used as an indicator of aerosol type. Four trajectory clusters (Midwest (MW), Southeast (SE), Southwest (SW) and Northwest (NW)) were identified as arriving at the site during the IOP (R. Ferrare, personal communication, 2004) using the NOAA HYSPLIT model [*Draxler and Hess*, 1998]. The SE air masses had the highest median scattering and absorption values and the

largest particles (on the basis of calculated geometric mean volume diameter from the GIF SMPS). These trajectories also had the highest median value of *g* (0.64) over the course of the study. The SE trajectories were associated with biomass burning events [*Gasparini et al.*, 2006]. *Wong and Li* [2002] have suggested that asymmetry parameters for heavy smoke plumes should be very small (*g* < 0.4), however, they were looking at fresh smoke plumes, while smoke arriving on the SE trajectory in this case has undergone long-range transport and is likely very different in size and composition from fresh smoke. The NW trajectory properties were the opposite of the SE trajectory with the lowest scattering and absorption observed, the smallest particles, and the lowest value of *g* (0.57). Median values of asymmetry parameter for the MW and SW trajectories were identical (0.61). (In these comparisons we just use the time period during the IOP when the GIF SMPS was operational (DOY 127–147)). For the four trajectory clusters the median single scattering albedo was very similar (ranged
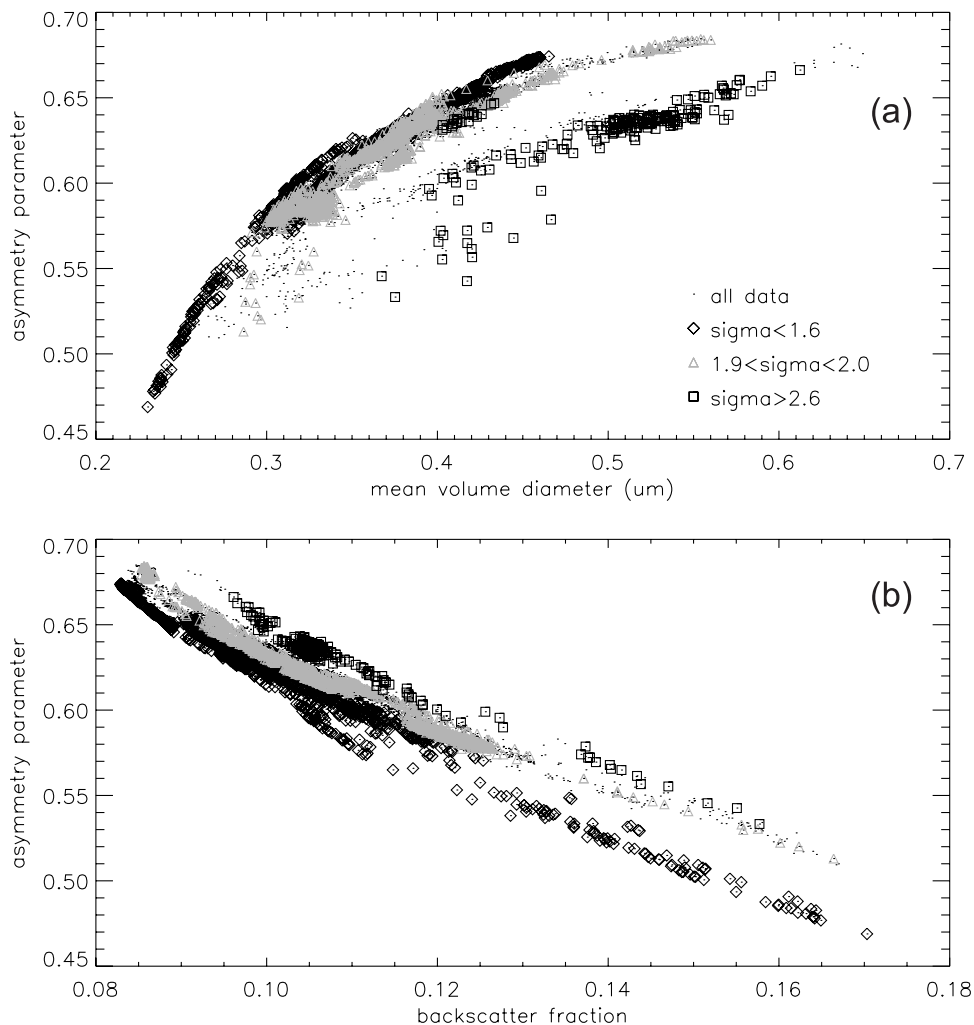
Figure 8. Importance of size distribution width. (a) Relationship between volume mean diameter and asymmetry parameter. (b) Relationship between backscatter fraction and asymmetry parameter. Data plotted are from AOS PCASP for diameter <1 μm, λ = 550 nm, and RI = 1.55 + 0.015i.

from 0.91 to 0.93) so the observed differences in g are likely due to differences in aerosol size rather than composition.

4.4. On the Basis of the Range of Aerosol Properties Observed During the Experiment, What Aerosol Properties Are Most Important to Measure to Obtain a Well-Constrained Value of g?

4.4.1. Aerosol Diameter

[53] The significant difference in g derived from the GIF Climet compared to the various other in situ instruments at the surface points to the importance of measuring the optically important aerosol in the accumulation mode (0.1 < Dp < 1.0 μm). While plots of the size distributions measured by the various instruments show excellent agreement in the GIF Climet's overlap size range (0.3–0.8 μm), the GIF Climet-derived asymmetry parameter is significantly higher because it is missing the contribution of the smaller particles (0.1–0.3 μm) which have a larger backscattering component and hence weight the asymmetry parameter toward lower values (e.g., equation (3)). Sensitivity tests using the GIF SMPS data show that, at SGP, including aerosol particles with diameter greater than 0.15 μm in the

Mie calculations will capture up to 95% of the asymmetry parameter's value.

[54] Figure 8a shows the relationship between asymmetry parameter and volume mean diameter calculated from the AOS PCASP size distribution measurements (Dp < 1 μm). Figure 8a shows that, while there is a general picture of increasing asymmetry parameter with increasing diameter, there are several groupings of points in the plot. These groupings appear to be related to the width of the aerosol size distribution (σ_g) which was calculated from the AOS PCASP data assuming a single mode, log normal volume size distribution could be fit to the measurements in the size range 0.1 μm < Dp < 1 μm. Figure 8b shows the relationship between asymmetry parameter and backscatter fraction for the same data set, also segregated by σ_g. Figure 8b suggests that as σ_g increases g also increases. For a constant value of backscattering fraction, there is less than a 5% change in g from σ_g < 1.6 to 1.9 < σ_g < 1.6 and likewise from 1.9 < σ_g < 1.6 to σ_g > 2.6. This is consistent with the analysis by *Marshall et al.* [1995] who modeled asymmetry parameter as a function of width of the size distribution as well as b and refractive index.

Table 5. Comparison of Calculated Asymmetry Parameters for GIF TDMA Assuming Constant Refractive Index Values and for Refractive Index Derived From Solubility Measurements

	g Range	g Median
$1.55 + 0.015i$ (dry)	$0.57 - 0.66$	0.63
Variable (dry)	$0.59 - 0.69$	0.65
$1.40 + 0.015i$ (wet)	$0.63 - 0.75$	0.69
Variable (wet)	$0.63 - 0.75$	0.70

[55] On the basis of the measured size distributions and estimated uncertainties in diameter for the GIF SMPS, the sensitivity of calculated asymmetry parameter to uncertainty in aerosol diameter for the SGP aerosol can be estimated. The diameter bins for the GIF SMPS were shifted by ±5 and ±10% while holding all other variables constant (e.g., wavelength and refractive index) to determine the effect of uncertainty in diameter on asymmetry parameter. A 5% change in diameter resulted in less than 2% change in calculated g; a 10% change in diameter resulted in less than a 5% change in calculated g. These changes are on the order of the overall variability of asymmetry parameter presented in Table 3.

4.4.2. Aerosol Composition (Based on Inferences From GIF TDMA Measurements)

[56] When constant composition is assumed for each solubility type (i.e., all solubility types have RI = 1.55 + 0.015i) there does not appear to be any sort of relationship between the volume contribution of various types of particles (soluble, mixed soluble, mixed insoluble or insoluble) and asymmetry parameter ($R^2 < 0.1$). Even when different compositions are assumed for the different solubility types, the relationship between volume contribution of the solubility types and asymmetry parameter is minimal. This is consistent with the idea that, for the most part, size is much more important than chemistry in determining asymmetry parameter. While Figure 5b, which shows the systematic relationship between single scattering albedo and asymmetry parameter for both the IOP and 8 years of SGP measurements (calculated using Henyey-Greenstein relationship), may suggest that there is an important compositional dependence for asymmetry parameter, it must be remem-

bered that small particles (dp < 0.2 μm) with nonzero imaginary refractive indices are strong absorbers and will also backscatter light efficiently [*Seinfeld and Pandis*, 1998]. Thus the systematic variation depicted in Figure 5 is a function of the aerosol size as well as its composition. One implication of Figure 5 is the importance of measuring the size dependence of absorbing aerosol. Figure 5 also suggests that the relative amount of scattering and absorption by the aerosol may be used to constrain assumptions about the value of the asymmetry parameter.

[57] For most of the comparisons in this paper a constant index of refraction was assumed. We investigated whether changes in the assumed dry particle refractive index resulted in a large change in calculated asymmetry parameter using the GIF TMDA data. Changing the dry index of refraction from 1.55 + 0.015i to 1.45 + 0.001i increased the calculated median asymmetry parameter by approximately 3% to 0.62. Changing the dry index of refraction to 1.60 + 0.04i decreased calculated asymmetry parameter by 2% to 0.59. Using more detailed chemical representation of the aerosol composition on a point by point basis (i.e., the solubility categories inferred from GIF TDMA size-resolved hygroscopic growth measurements (Gasparini et al., submitted manuscript, 2005)) results in 3% difference in median values of asymmetry parameter (Table 5) compared to the use of a constant index of refraction.

[58] The underlying assumption of basic Mie theory (i.e., homogeneous spheres) in all derivations of g presented here represents a possible departure from actual particle properties, include the mixing state of the aerosol and aerosol shape. Work by *Lesins et al.* [2002] and *Gonzalez-Jorge and Ogren* [1996] suggest that neither of these factors will have much influence on the calculated asymmetry parameter. However, other optical properties such as extinction and single scattering albedo may be more affected by assumptions about mixing state and/or shape.

4.5. Are There Any Significant Differences in the Estimate of g for Surface-Based Versus Vertical Profile Measurements?

[59] Figure 9a shows dry asymmetry parameters derived from equation (4) for both the AOS and IAP nephelometers.
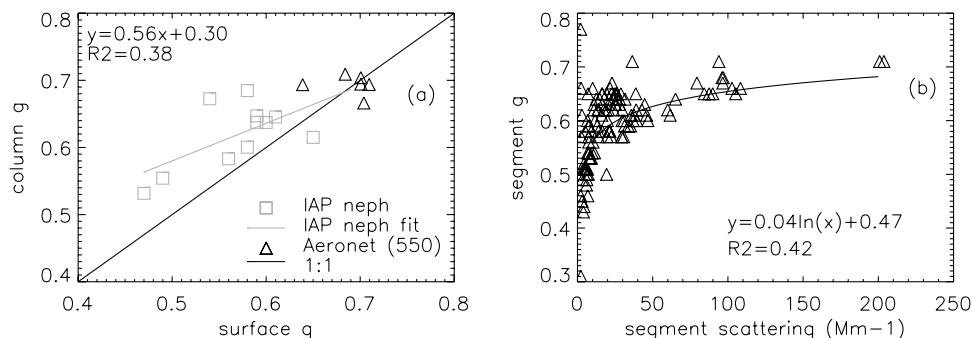

Figure 9. (a) Surface g (shaded) based on measurements from the AOS nephelometer and equation (4) versus column average g based on g calculated for individual flight layers from the IAP nephelometer and equations (4) and (5) and surface g (solid) based on GIF TDMA measurements at high humidity compared to AERONET g at ambient conditions. (b) Systematic relationship between segment averaged light scattering and segment asymmetry parameter from IAP nephelometer. (Note that removal of the two high scattering values lowers R^2 to 0.39 and removal of lowest g value lowers R^2 to 0.41.)

The surface value is the asymmetry parameter averaged over the typical 2 hour IAP flight time. The column values for g come from applying equation (5) to asymmetry parameters calculated for each flight level. There is not a strong relationship between the surface and column values of g ($R^2 = 0.38$). There is no correlation ($R^2 < 0.05$) between g derived from high humidity GIF TDMA measurements at the surface and AERONET, although the points do cluster around the 1:1 line (Figure 9a). Aside from the low number of data points, this lack of agreement is not surprising given that more than 80% of the profile flights during the IOP exhibited a layer of aerosol above the surface. From Figure 9a it also appears that derived values of the asymmetry parameter may be higher aloft than at the surface. This seems odd as larger values of asymmetry parameter tend to correspond with larger diameter particles which intuition suggests should be closer to the surface. Figure 9b shows a systematic relationship between increasing light scattering and asymmetry parameter when the data are plotted for all the flight levels. This implies that the cause of the column-averaged g being larger than the surface g may be due to the influence of the elevated layers of aerosol.

4.6. Are the g Values Observed During This Study Typical of Conditions at the Site?

[60] Here we just consider whether g is representative of typical conditions at the site. The median asymmetry parameter derived from equation (4) for dry conditions (0.59) was quite similar (within 2%) to the long-term values, despite increased amounts of aerosol at the site during the IOP and somewhat lower single scattering albedo. The Ångström exponent during the IOP was also similar to long-term values. These observations are consistent with the contention that aerosol size is the most important parameter influencing derived asymmetry parameter.

[61] For high-humidity conditions (for simplicity we use RH = 85% rather than ambient RH), the AOS nephelometer-derived asymmetry parameter during the IOP (0.73) is significantly lower (8%) than calculated for the long-term data set (long term g at RH = 85% is 0.79). The low asymmetry values for the IOP are most likely attributable to less aerosol growth due to lower aerosol hygroscopicity: The f(RH) values during the IOP were significantly lower (1.43) than the long-term f(RH) median value (1.68) suggesting the IOP aerosol was less hygroscopic. Thus, for deriving a reasonable value of asymmetry parameter for nondry conditions the two most influential factors are (1) dry size distribution and (2) how the aerosol changes with relative humidity.

5. Conclusions

[62] A month-long field experiment in Oklahoma provided a large aerosol data set with numerous types of measurements from which aerosol optical properties, Mie-equivalent asymmetry parameter in particular, were derived. The main objective was to determine the value and range of asymmetry parameter at the site. Using five different methods (Henyey-Greenstein approximation, Mie theory, the King inversion, results from the Dubovik inversion algorithm and the new Fiebig inversion method) values for dry and

ambient asymmetry parameter were derived from the suite of in situ and remote measurement data available from the field experiment. These derived values of g at 550 nm ranged from 0.60 (±0.03) for dry aerosol to 0.65 (±0.05) for aerosol at ambient conditions. Calculations of radiative forcing over the range of observed asymmetry parameter showed that a 10% decrease in g corresponded to a 19% reduction in radiative forcing at the top of the atmosphere and a 13% reduction at the surface. Investigation of the factors controlling the value of the asymmetry parameter suggested that aerosol size distribution, specifically in the accumulation mode ($0.1 < dp < 1.0$ µm) was the most important parameter to measure. Aerosol composition was important mainly in how it controlled the hygroscopic growth (i.e., size) of the particles.

References

Anderson, T. L., and J. A. Ogren (1998), Determining aerosol radiative properties using the TSI 3563 integrating nephelometer, *Aerosol Sci. Technol.*, *29*, 57–59.

Anderson, T. L., S. J. Masonis, D. S. Covert, N. C. Ahlquist, S. G. Howell, A. D. Clarke, and C. S. McNaughton (2003), Variability of aerosol optical properties derived from in situ aircraft during ACE-Asia, *J. Geophys. Res.*, *108*(D23), 8647, doi:10.1029/2002JD003247.

Andrews, E., P. J. Sheridan, J. A. Ogren, and R. Ferrare (2004), In situ aerosol profiles over the Southern Great Plains CART site: 1. Aerosol optical properties, *J. Geophys. Res.*, *109*, D06208, doi:10.1029/2003JD004025.

Bond, T. C., T. L. Anderson, and D. Campbell (1999), Calibration and intercomperison of filter-based measurements of visible light absorption by aerosols, *Aerosol Sci. Tech.*, *30*, 582–600.

Boucher, O. (1998), On aerosol direct shortwave forcing and the Henyey-Greenstein phase function, *J. Atmos. Sci.*, *55*, 128–134.

Charlson, R. J., W. M. Porch, A. P. Waggoner, and N. C. Ahlquist (1974), Background aerosol light scattering characteristics: Nephelometric observations at Mauna Loa Observatory compared with results at other remote locations, *Tellus*, *26*, 345–360.

Charlson, R. J., J. Lagner, H. Rodhe, C. B. Leovy, and S. G. Warren (1991), Perturbation of the northern hemisphere radiative balance by backscattering from anthropogenic sulfate aerosols, *Tellus, Ser. AB*, *43*, 152–163.

Clarke, A. D., et al. (2002), INDOEX aerosol: A comparison and summary of chemical, microphysical, and optical properties observed from land, ship, and aircraft, *J. Geophys. Res.*, *107*(D19), 8033, doi:10.1029/2001JD000572.

d'Almeida, G. A., P. Koepke, and E. P. Shettle (1991), *Atmospheric Aerosols: Global Climatology and Radiative Characteristics*, A. Deepak, Hampton, Va.

Delene, D., and J. A. Ogren (2002), Variability of aerosol optical properties at four North American surface monitoring sites, *J. Atmos. Sci.*, *59*, 1135–1150.

Draxler, R. R., and G. D. Hess (1998), An overview of the Hysplit_4 modeling system for trajectories, dispersion, and deposition, *Aust. Meteorol. Mag.*, *47*, 295–308.

Dubovik, O., and M. D. King (2000), A flexible inversion algorithm for retrieval of aerosol optical properties from Sun and sky radiance measurements, *J. Geophys. Res.*, *105*(D16), 20,673–20,696.

Dubovik, O., A. Smirnov, B. N. Holben, M. D. King, Y. J. Kaufman, T. F. Eck, and I. Slutsker (2000), Accuracy assessment of aerosol optical properties retrieval from AERONET sun and sky radiance measurements, *J. Geophys. Res.*, *105*(D8), 9791–9806.

Eck, T. F., B. N. Holben, O. Dubovik, A. Smirnov, I. Slutsker, J. M. Lobert, and V. Ramanathan (2001), Column-integrated aerosol optical properties over the Maldives during the northeast monsoon for 1998–2000, *J. Geophys. Res.*, *106*(D22), 28,555–28,566.

Ferrare, R., et al. (2006), The Atmospheric Radiation Measurement Program May 2003 Intensive Operations Period examining aerosol properties and radiative influences: Preface to special section, *J. Geophys. Res.*, doi:10.1029/2005JD006908, in press.

Fiebig, M., C. Stein, F. Schroder, P. Feldpausch, and A. Petzold (2005), Inversion of data containing information on the aerosol particle size distribution using multiple instruments, *J. Aerosol Sci.*, *36*(11), 1353–1372.

Formenti, P., M. O. Andreae, and J. Lelieveld (2000), Measurements of aerosol optical depth above 3570 m asl in the North Atlantic free troposphere: Results from ACE-2, *Tellus, Ser. B*, *52*, 678–693.

Gasparini, R., R. Li, and D. R. Collins (2004), Integration of size distributions and size-resolved hygroscopicity measured during the Houston Supersite for compositional categorization of the aerosol, *Atmos. Environ.*, *38*, 3285–3303.

Gasparini, R., R. Li, D. R. Collins, and R. A. Ferrare (2006), Application of aerosol hygroscopicity measured at the ARM Southern Great Plains site to examine composition and evolution, *J. Geophys. Res.*, doi:10.1029/2004JD005448, in press.

Gayet, J. F., F. Auriol, S. Oshchepkov, F. Schroder, C. Duroure, G. Febvre, J. F. Fournol, O. Creel, P. Personne, and D. Daugereon (1998), In situ measurements of the scattering phase function of stratocumulus contrails and cirrus, *Geophys. Res. Lett.*, *25*, 971–974.

Gerber, H., Y. Takano, T. J. Garrett, and P. V. Hobbs (2000), Nephelometer measurements of the asymmetry parameter, volume extinction coefficient and backscatter ration in Arctic clouds, *J. Atmos. Sci.*, *57*, 3021–3034.

Gonzalez-Jorge, H. G., and J. A. Ogren (1996), Sensitivity of retrieved aerosol properties to assumptions in the inversion of spectral optical depths, *J. Atmos. Sci.*, *53*, 3669–3683.

Hand, J. L., and S. M. Kreidenweis (1996), Size corrections based on refractive index for Particle Measurements Systems active scattering aerosol sizing probe, CIRA report, Colo. State Univ., Fort Collins.

Hartley, W. S., and P. V. Hobbs (2001), An aerosol model and aerosol-induced changes in the clear-sky albedo off the east coast of the United States, *J. Geophys. Res.*, *106*(D9), 9733–9748.

Haywood, J. M., and K. P. Shine (1995), The effect of anthropogenic sulfate and soot aerosol on the clear sky planetary radiation budget, *Geophys. Res. Lett.*, *22*, 603–606.

Hegg, D. A., and H. Jonsson (2000), Aerosol number-to-volume relationship and relative humidity in the eastern Atlantic, *J. Geophys. Res.*, *105*(D2), 1987–1995.

Heintzenberg, J., and R. J. Charlson (1996), Design and applications of the integrating nephelometer: A review, *J. Atmos. Oceanic Technol.*, *13*, 987–1000.

Hess, M., P. Koepke, and I. Schult (1998), Optical properties of aerosols and clouds: The software package OPAC, *Bull. Am. Meteorol. Soc.*, *79*, 831–844.

Intergovernmental Panel on Climate Change (2001), *Climate Change 2001: The Scientific Basis*, edited by J. T. Houghton et al., Cambridge Univ. Press, New York.

King, M. D. (1982), Sensitivity of constrained linear inversions to the selection of the Lagrange multiplier, *J. Atmos. Sci.*, *39*, 1356–1369.

King, M. D., D. M. Byrne, B. M. Herman, and J. A. Reagan (1978), Aerosol size distributions obtained by inversion of spectral optical depth measurements, *J. Atmos. Sci.*, *35*, 2153–2167.

Kotchenruther, R. A., and P. V. Hobbs (1998), Humidification factors of aerosols from biomass burning in Brazil, *J. Geophys. Res.*, *103*(D24), 32,081–32,089.

Leong, K. H., M. R. Jones, D. J. Holdridge, and M. Ivey (1995), Design and test of a polar nephelometer, *Aerosol Sci. Technol.*, *23*, 341–356.

Lesins, G., P. Chylek, and U. Lohmann (2002), A study of internal and external mixing scenarios and its effect on aerosol optical properties and direct radiative forcing, *J. Geophys. Res.*, *107*(D10), 4094, doi:10.1029/2001JD000973.

Liu, P. S. K., W. R. Leaitch, J. W. Strapp, and M. A. Wasey (1992), Response of particle measuring systems airborne ASASP and PCASP to NaCl and latex particles, *Aerosol Sci. Technol.*, *16*, 83–95.

Marshall, S. F., D. S. Covert, and R. J. Charlson (1995), Relationship between asymmetry parameter and hemispheric backscatter ratio: Implications for climate forcing by aerosols, *Appl. Opt.*, *34*(27), 6306–6311.

Ogren, J. A. (1995), In situ observations of aerosol properties, in *Aerosol Forcing of Climate*, edited by R. J. Charlson and J. Heintzenberg, pp. 215–226, John Wiley, Hoboken, N. J.

Ricchiazzi, P., S. Yang, C. Gautier, and D. Sowle (1998), SBDART: A research and teaching software tool for plane-parallel radiative transfer in the Earth's atmosphere, *Bull. Am. Meteorol. Soc.*, *79*, 2101–2114.

Ross, J. L., P. V. Hobbs, and B. Holben (1998), Radiative characteristics of regional hazes dominated by smoke from biomass burning in Brazil: Closure tests and direct radiative forcing, *J. Geophys. Res.*, *103*(D24), 31,925–31,941.

Schmid, B. (2004), Measurement and modeling of vertically resolved aerosol optical properties and radiative fluxes over the ARM SGP site during the May 2003 Aerosol IOP, paper presented at 14th ARM Science Team Meeting, U. S. Dep. of Energy, Albuquerque, N. M., 22–26 March.

Schmid, B., et al. (2006), How well do state-of-the-art techniques measuring the vertical profile of tropospheric aerosol extinction compare?, *J. Geophys. Res.*, doi:10.1029/2004JD005837, in press.

Seinfeld, J. H., and S. N. Pandis (1998), *Atmospheric Chemistry and Physics*, John Wiley, Hoboken, N. J.

Sheridan, P. J., D. J. Delene, and J. A. Ogren (2001), Four years of continuous surface aerosol measurements from the Department of Energy's Atmospheric Radiation Measurement Program Southern Great Plains Cloud and Radiation Testbed site, *J. Geophys. Res.*, *106*(D18), 20,735–20,747.

Sheridan, P. J., A. Jefferso, and J. A. Ogren (2002), Spatial variability of submicrometer aerosol radiative properties over the Indian Ocean during INDOEX, *J. Geophys. Res.*, *107*(D19), 8011, doi:10.1029/2000JD000166.

Volten, H., O. Munoz, E. Rol, J. F. De Haan, W. Vassen, J. W. Hovenier, K. Muinonen, and T. Nousianinen (2001), Scattering matrices of mineral aerosol particles at 441 and 632.8 nm, *J. Geophys. Res.*, *106*, 17,375–17,401.

Wang, J., et al. (2002), Clear-column radiative closure during ACE-Asia: Comparison of multiwavelength extinction derived from particle size and composition with results from Sun photometry, *J. Geophys. Res.*, *107*(D23), 4688, doi:10.1029/2002JD002465.

Wang, J., R. C. Flagan, and J. H. Seinfeld (2003), A differential mobility analyzer (DMA) system for submicron aerosol measurements at ambient relative humidity, *Aerosol Sci. Technol.*, *37*(1), 46–52.

Wiscombe, W. J., and G. W. Grams (1976), The backscattered fraction in two-stream approximations, *J. Atmos. Sci.*, *33*, 2440–2451.

Wong, J., and Z. Li (2002), Retrieval of optical depth for heavy smoke aerosol plumes: Uncertainties and sensitivities to optical properties, *J. Atmos. Sci.*, *59*, 250–261.

————————

E. Andrews and A. McComiskey, Cooperative Institute for Research in Environmental Sciences, University of Colorado, Boulder, CO 80305, USA. (betsy.andrews@noaa.gov)

P. Arnott, Desert Research Institute, Reno, NV 89512, USA.

D. Collins, Department of Atmospheric Sciences, Texas A&M University, College Station, TX 77843, USA.

D. Covert and R. Elleman, Department of Atmospheric Sciences, University of Washington, Seattle, WA 98195, USA.

M. Fiebig, Institut für Physik der Atmosphäre, Deutsches Zentrum für Luft- und Raumfahrt Oberpfaffenhofen, D-82234 Wessling, Germany. (markus.fiebig@dlr.de)

R. Gasparini, Source Environmental Sciences, Inc., 4100 Westheimer, Suite 106, Houston, TX 77027, USA. (enviroberto@yahoo.com)

H. Jonsson, Center for Interdisciplinary Remotely-Piloted Aircraft Studies, Naval Postgraduate School, Marina, CA 93933, USA.

J. A. Ogren and P. J. Sheridan, Global Monitoring Division, NOAA Earth System Research Laboratory, Boulder, CO 80309, USA.

B. Schmid, Bay Area Environmental Research Institute, Sonoma, CA 95476, USA.

J. Wang, Brookhaven National Laboratory, Upton, NY 11973, USA.